To be published in *Geophysical Research Letters*
Geophys. Res. Lett. 40(23) 6059-6063 2013

Fault frictional parameters and material properties revealed by slow slip events at Kilauea volcano, Hawai‘i

James H. Foster[1], Anthony R. Lowry[2], Benjamin A. Brooks[1, 3]
[1]SOEST, University of Hawai‘i, 1680 East–West Rd, Honolulu, HI 96822
[2]Department of Geology, Utah State University, 4505 Old Main Hill, Logan, UT 84322
[3] *now at* USGS, 345 Middlefield Rd., MS 977 Menlo Park, CA 94025

Abstract
We categorize slow slip events at Kilauea Volcano into two distinct families based on GPS measurements of the surface displacement patterns. An event correlation filter confirms that “eastern” and “western” families are statistically distinguishable, with the western family notably self-similar. The western family exhibits quasi-periodicity with regular repeat times, while eastern family events are aperiodic or have complicated periodicity. If the decollement is the source fault for both families of events, it must have varying frictional properties at the ~10 km scale of separation. The temporal slip and spatial scaling behavior are consistent with a simplistic rate- and state-dependent frictional formalism provided that the characteristic slip distance for state evolution, D_c, is of order mm rather than the 10–100 μm typically found in lab studies, and the shear rigidity is around 2 GPa, consistent with fault gouge material.

1. Introduction
The proliferation of dense continuous GPS (CGPS) networks has demonstrated that a large portion of aseismic fault slip occurs episodically in the form of slow slip events (SSEs) [*Schwartz and Rokosky*, 2007]. SSEs have been observed mostly in subduction zones; in strike slip faults observed SSEs are rare. Because SSEs redistribute stresses on faults with large earthquake (EQ) and often tsunamigenic potential, it is critical to understand their phenomenology and role in these systems.

Emerging theories of slow slip at subduction zones [*Liu and Rice*, 2005; 2007; *Rubin*, 2008; 2011; *Segall et al.*, 2010] indicate they may occur preferentially near a zone of frictional transition from velocity-strengthening (“stable”) to velocity-weakening (“stick-slip”). Explorations of “rate- and state-dependent” (R&S) frictional formulations find complicated slip patterns [*Liu and Rice*, 2007] that reproduce many of the characteristics of observed SSEs. One important outcome is that fault patches may have intrinsic resonance periods controlled by frictional parameters [*Lowry*, 2006; *Perfettini and Schmittbuhl*, 2001; *Perfettini et al.*, 2001], at which small perturbing stresses may elicit strong quasi-periodic slips. Consequently, the characteristics of observed quasi-periodic SSEs may be used to infer information about the fault frictional parameters.

For subduction zone SSEs, the frictional transition zone is located down-dip of the locked seismogenic zone. Although the up-dip portion of some subduction zone faults may also produce SSEs [e.g. *Davis et al.*, 2011], Kilauea’s mobile south flank is the only location where up-dip SSEs have been confirmed, and in fact this appears to be the sole source zone for SSEs detected here (Figure 1). During the past 17 years at least ten Kilauea SSEs have been identified from CGPS data [*Brooks et al.*, 2006; *Brooks et al.*, 2008; *Cervelli et al.*, 2002; *Montgomery-Brown et al.*, 2009; *Segall et al.*, 2006] with surface displacements up to a few cms and duration of several hours to two days. The source-network geometry does not resolve fault depth well [*Brooks et al.*, 2006], but recent studies of triggered seismicity [*Segall et al.*, 2006] and layered rheology [*Montgomery-Brown et al.*, 2009] conclude that the basal decollement is the most likely source location. Deformation monitoring suggests the inland portion of the decollement near the rift zones creeps while the portion below the coastline remains locked. Accumulated stresses are relieved by large EQs, such as the 1868 M 7.9 Kau and 1975 M_w 7.7 Kalapana events. SSEs add extra complexity to this system, representing an additional mode of accommodation to the stresses in the flank. Using CGPS data, we show that the catalog of Kilauea SSEs can be categorized as two "families" with distinctive spatial and quasi-periodic temporal characteristics.

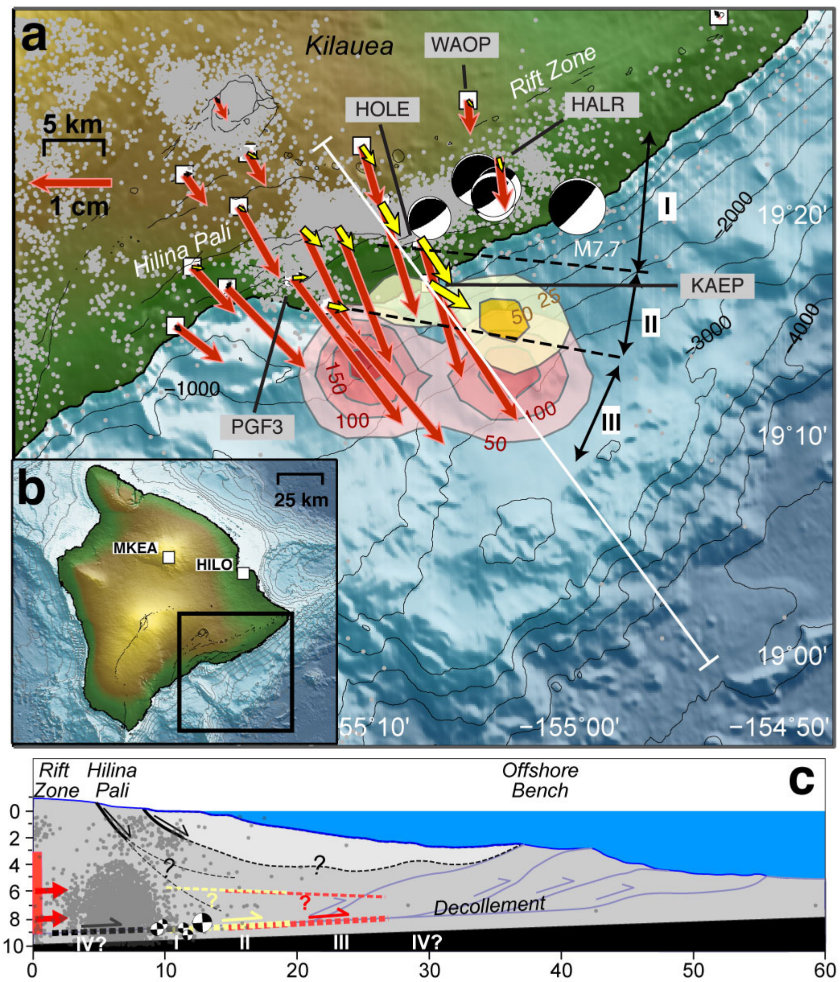

Figure 1. a) Mean SSE slip for each family (red=WF; yellow=EF). Centroid moment tensors for M_w5+ EQs since 1975 are lower hemisphere projections (black = compression). All EQs since 1997 in the depth range 5-15 km are shown as gray dots. White line indicates cross-section shown in c). Dashed blank lines separate the zones of stick-slip (I), complex-periodic/aperiodic (II) and simple periodic (III) slip behavior. b) Big Island of Hawaii showing Kilauea location. c) Schematic cross section. Heavy dashed yellow and red lines indicate most likely source region for EF/WF SSEs, light dashed lines indicate range of depths consistent with geodetic data [*Brooks et al.*, 2006]. CMTs shown from the cross-section perspective.

2. Two Families of Slow Slip Events

Kilauea's SSE displacement vectors can be categorized into "western" and "eastern" families (Figure 1). The western family (WF) forms a "bow"-shaped distribution of displacement vectors, with the maximum displacement located around station PGF3. The eastern family (EF) shows either randomly-oriented, statistically insignificant displacements, or very small displacements to the east for western CGPS sites. Maximum measured EF displacements are located at or around HOLE or KAEP, although, as the network does not sample the coastal plane to the east of these sites the location of maximum displacement, and the easterly limit of significant motions is poorly constrained.

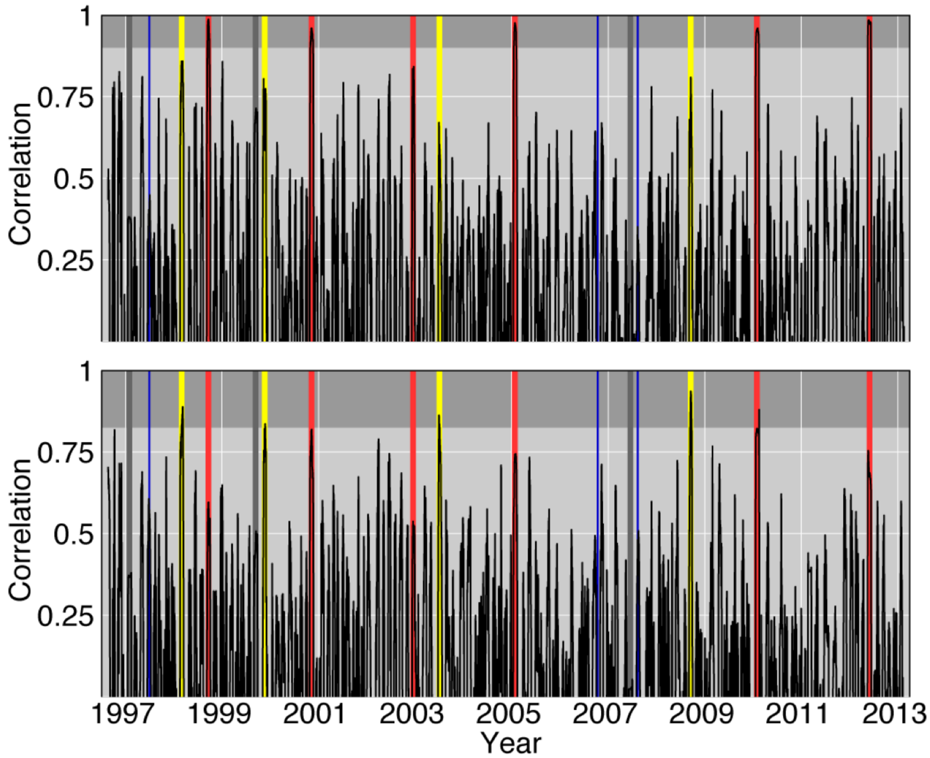

Figure 2. Correlations of daily estimated network slips estimated with respect to a) reference WF event and b) reference EF event. Red/yellow bars mark WF/EF events. Dark gray vertical lines indicate dike intrusions or significant (M>=5.0) EQs. Dark horizontal band = 90%/80% correlation zone for the WF and EF respectively.

We distinguish the two families quantitatively with an event-categorization filter [e.g. *Montgomery-Brown et al.*, 2009]. A reference event, *j*, for each family is created from the normalized 3-D displacements for each site for that family's events. Incremental displacements, *i*, are estimated by fitting steps functions at each epoch (see description in Auxiliary Material). The correlation, c_{ij}, between them is given by

$$c_{ij} = \frac{|i.j|}{\sqrt{|i.i| \times |j.j|}}$$

The c_{ij} time series (Figure 2) confirms high correlation peaks associated with each of the identified events (Figure 2a) in the WF. The 2007 event is overprinted by a diking event, but residual vectors strongly indicate WF type slip [*Brooks et al.*, 2008; *Montgomery-Brown et al.*, 2010]. The Dec 2002 event has a relatively low correlation reflecting its small magnitude and activation of only the western-most CGPS sites. The EF (Figure 2b) events show lower correlations, suggesting greater heterogeneity and/or lower signal-to-noise ratio. The EF filter also identifies a previously unrecognized event on 17 Sep 2008. Its maximum slip vectors are statistically significant, and the high spatial correlation suggests that this is an EF SSE. With our time-series and methodology, we are unable to resolve the additional possible events identified by Montgomery-Brown et al [2009], and we restrict our catalog to eleven clearly identified events: four EF (including the newly recognized 2008 SSE), and seven WF events (see Auxiliary Materials Figures FS01-FS02).

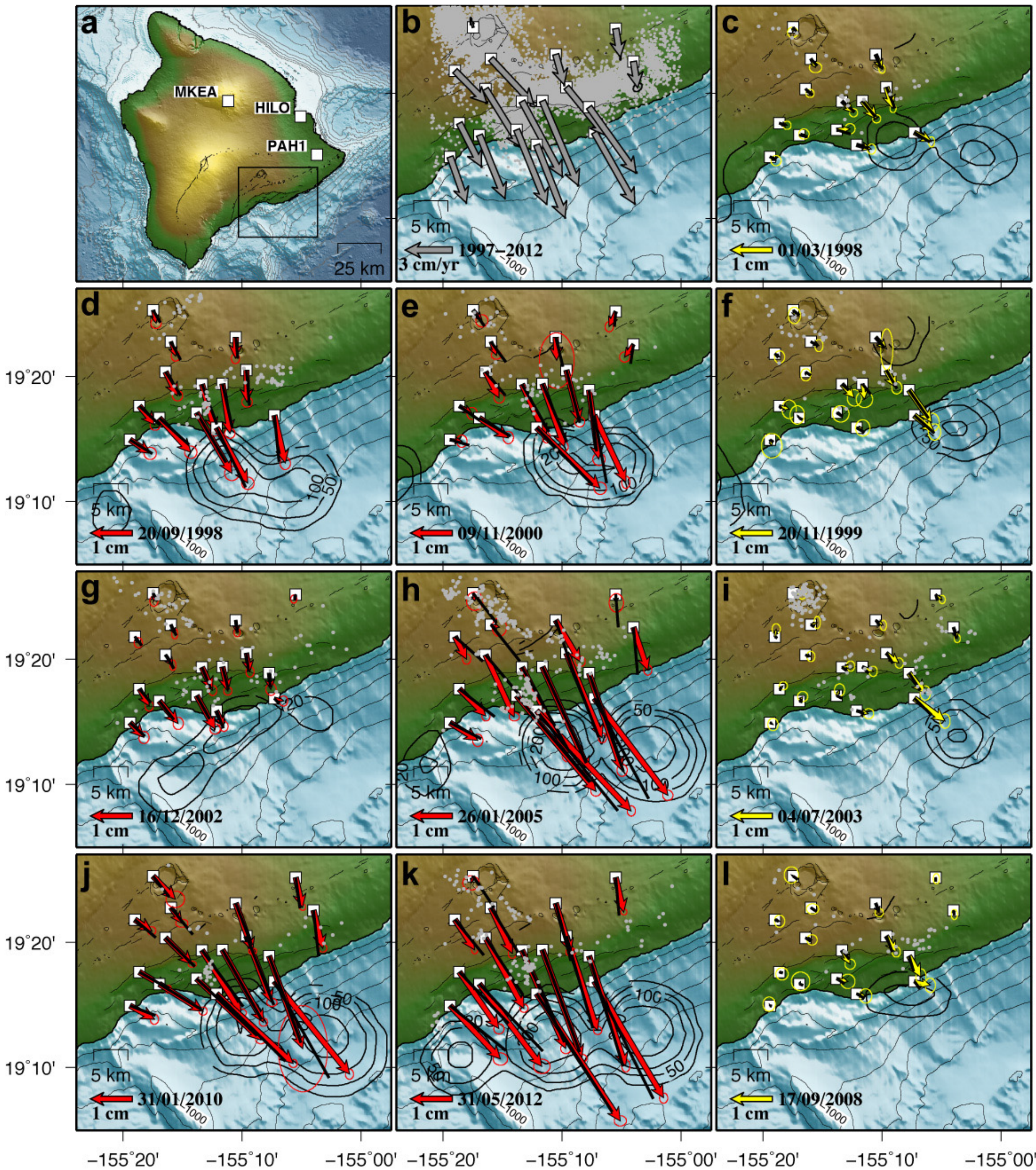

Figure FS01. a) Big Island and location of Kilauea south flank. b) Continuous creep displacement rates for 1997-2012. c)-l) All recognized (except for June 2007 west family event masked by dike intrusion) west (red) and east (yellow) SSE events with modeled slip distributions (black contours) and model displacements (blank vectors). Earthquakes for the 3 day window either side of each event are shown in gray dots.

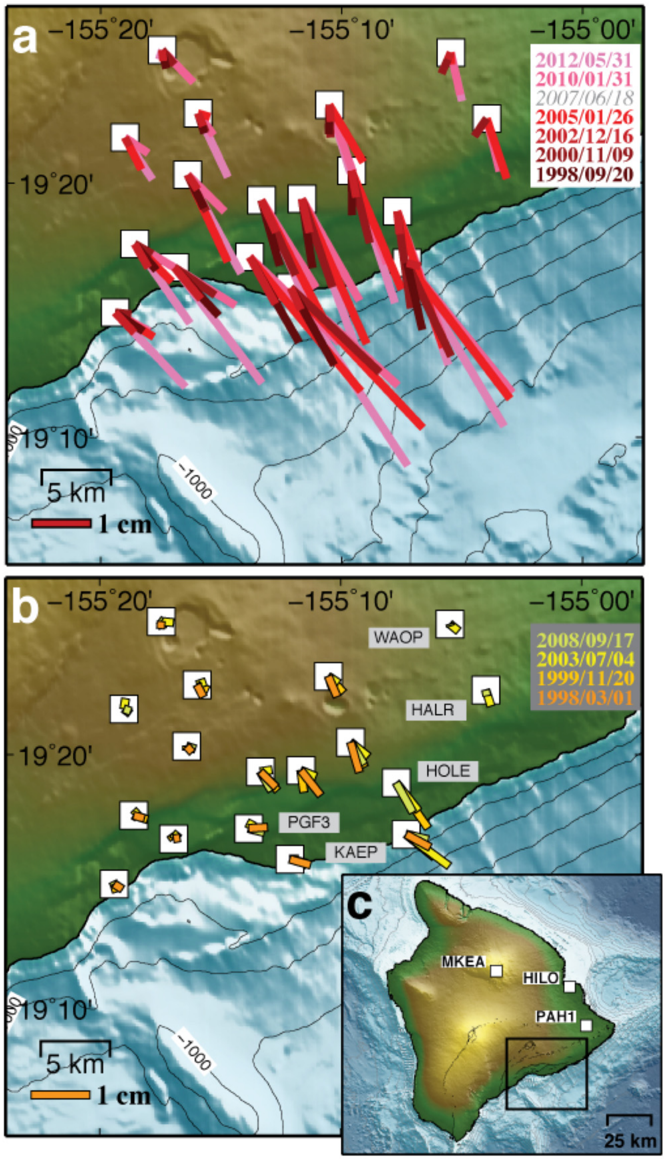

Figure FS02: Network slips for all SSEs we identify (except the June 2007 west family event which is overprinted by a dike event). a) West family events, b) East family events. c) Big Island of Hawaii, showing location for network slip maps.

3. Slip Characteristics

The repeat times between events for each family reveal very different patterns (Figure 3). Although the sequences of events are not notably time or slip predictable in the traditional sense, the recurrence intervals for the WF are extremely regular with an average of 834 +/- 75 days. The EF events on the other hand show little regularity: their average recurrence time is 1284 +/- 637 days. However, the 629, 1322, and 1902-day intervals between the 4 events are multiples of 0.98, 2.06, and 2.96 times 642 days. While there is no evidence of any unrecognized SSE events on the “missing” dates this implies, it raises the intriguing possibility of an, as yet unresolved, and perhaps complex, periodicity for the EF SSEs.

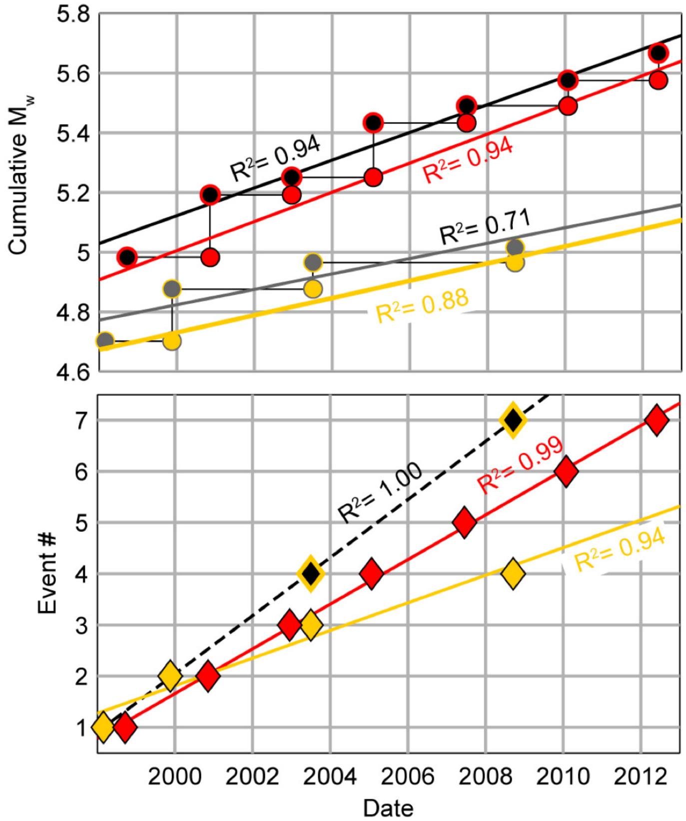

Figure 3. Top: Time- and slip-predictability plot of cumulative M_w for each family of events. Red/yellow dots indicate the WF/EF events. Bottom: Non-parametric representation of event family repeatabilities. The WF shows strong quasi-periodicity. The EF does not (yellow), unless a complex periodicity or undetected events are proposed (black/yellow).

The distinct SSE families suggest activation of distinct fault patches. We explore this by solving for the slip distribution, assuming each involves slip on the decollement with the same dip-slip fault motion (see Auxiliary Materials). The mean slip for each family is shown in Figure 1. The WF and EF involve discrete patches of the fault plane, though this inversion indicates some overlap between the seaward extent of EF slip and the easternmost extent of WF slip patches. Notably, each WF-EF event-pair involves two discrete patches with one patch displaced seaward and eastward of the other. Although the size of each patch imaged using this inversion approach is largely controlled by the choice of smoothing factor (see Aux. Mat.), the resolution of distinct WF and EF patches suggests variability on the fault plane at a spatial scale of ~10 km. Moment magnitude (M_w) ranges for the two families are also distinct: EF events have M_w 5.4 +/- 0.2 and WF 5.8+/- 0.3.

3. Frictional Parameters and Material Properties

The differences in period and regularity of recurrence, and in magnitudes and locations of slip, indicate that either the stressing rates or the fault frictional properties, or both, vary significantly. Observed inter-event displacement rates show little change along-strike [*Owen et al.,* 2000], indicating constant stress rate. Liu and Rice [2005, 2007] modeled a R&S formulation of a subduction megathrust to find that, depending on the specific combinations of effective normal stress and fault frictional parameters, fault responses at the frictional transition zone range from stick-slip, through complex- or aperiodic transients, to periodic slip and finally to continuous creep. This spectrum of responses strongly resembles the observed phenomenology of slip behavior on the south flank (Figure 1): the cloud of microearthquakes near the decollement, and the centroid locations for all major M5+ EQs recorded in the last 40 years, delineate a locked, stick-slip frictional regime. The source regions for the EF and WF SSEs exhibit aperiodicity (or complex periodicity) and simple periodicity respectively. The geometry of the slip observations limits the resolution of the seaward and eastward edges of the SSE nucleation zones, but it seems reasonable to assume that in the distal regions, the fault frictional regime produces continuous creep.

The Dieterich R&S formulation of frictional slip defines shear stress τ as the product of effective normal stress $\sigma_e = \sigma_n - p$ (where p is pore pressure) and a friction coefficient μ, which follows the slip rate (V) and state (θ) law:

$$\tau = \sigma_e \mu = \sigma_e \left[\mu_0 + a \ln\left(\frac{V}{V_0}\right) + b \ln\left(\frac{V_0 \theta}{D_c}\right) \right],$$

where a, b, and D_c are experimentally determined material constants, μ_0 is the static coefficient of friction, and V_0 is a normalizing velocity. Laboratory experiments suggest a and b are ~0.01 with $a - b < 0$ defining a velocity weakening frictional regime. For regimes where SSEs occur, the ratio a/b is expected to exceed 0.9. Values for D_c determined from laboratory experiments are typically ~10 μm for granitic rocks, with values as high as 100 μm found for fault gouge. With this formulation for the fault friction, and assuming an age law for the state parameter, it can be shown that a fault (segment) at its critical stiffness has a resonant response at a critical period [*Perfettini and Schmittbuhl*, 2001]:

$$T_c = \frac{2\pi D_c}{V_{creep}} \sqrt{\frac{a}{b-a}}, \tag{1}$$

where V_{creep} is the steady state creep of the fault. In the case of the WF, this critical period is well defined at 834 days and the recent aseismic creep rate of the south flank has been modeled at V_{creep} ~0.25 m/yr [*Owen et al.*, 2000] or ~8 x 10^{-9} m s^{-1}.

R&S models also imply intrinsic length scales for fault slip. The half-length of the minimum available patch size required to nucleate a slip event, h^*, is given by [*Rice*, 1993; *Rubin*, 2008]:

$$h^* \equiv \frac{G' D_c}{(b-a)\sigma_e},$$

where G' is the effective shear modulus given by $G/(1-\nu)$ in which G is the shear modulus and ν Poisson's ratio. A second scale defines the half-length of the limiting patch size for stability. If the available fault length exceeds a critical value, a nucleating slip event will accelerate into an EQ. For a SSE governed solely by R&S friction to remain stable, the fault length must be smaller than $2L_\infty$ [*Rubin and Ampuero*, 2005] where

$$L_\infty \equiv \frac{G' D_c b}{\pi \sigma_e (b-a)^2}.$$

A final equation relates the dip-direction length-scale to slip during SSEs [*Rubin*, 2008]:

$$W = \frac{u_{SSE} G'}{\beta \sigma_e (b-a) \ln\left(V_{SSE} / V_{creep} \right)},$$

where β is an empirical constant of order 1, u_{SSE} is slip amount, and V_{SSE} is the slip speed during the SSE. Along with these theoretical length scales, we have some observational length scale constraints. The geometry of the entire flank provides a maximum length scale of ~40km (which may be less than the critical $2L_\infty$ for the SSE patches). Although parts of the flank can nucleate seismic events, the SSEs have not accelerated into regular EQs. This provides a constraint on the portion of the fault(s) slipping with each SSE family: $2h^* < W < 2L_\infty$. If both families of events involve slip on the same fault plane, the ~5-10 km distance between the two SSE families' slip patches provides an additional length scale constraint.

The WF SSE slip distribution has mean u_{SSE} = 0.06 m, which appears to accrue at a roughly linear rate over ~2 days [*Montgomery-Brown et al*, 2009; *Segall et al.*, 2006; *Cervelli et al.*, 2002], giving $V_{SSE} = 3.5 \times 10^{-7}$ m s^{-1}. Using parameter values defined above (Auxiliary Material Table TS02), and setting β = 1 [*Rubin*, 2008], these relations allow us to explore order-of-magnitude ranges for the frictional parameters and *G'* of the offshore portion of Kilauea's decollement.

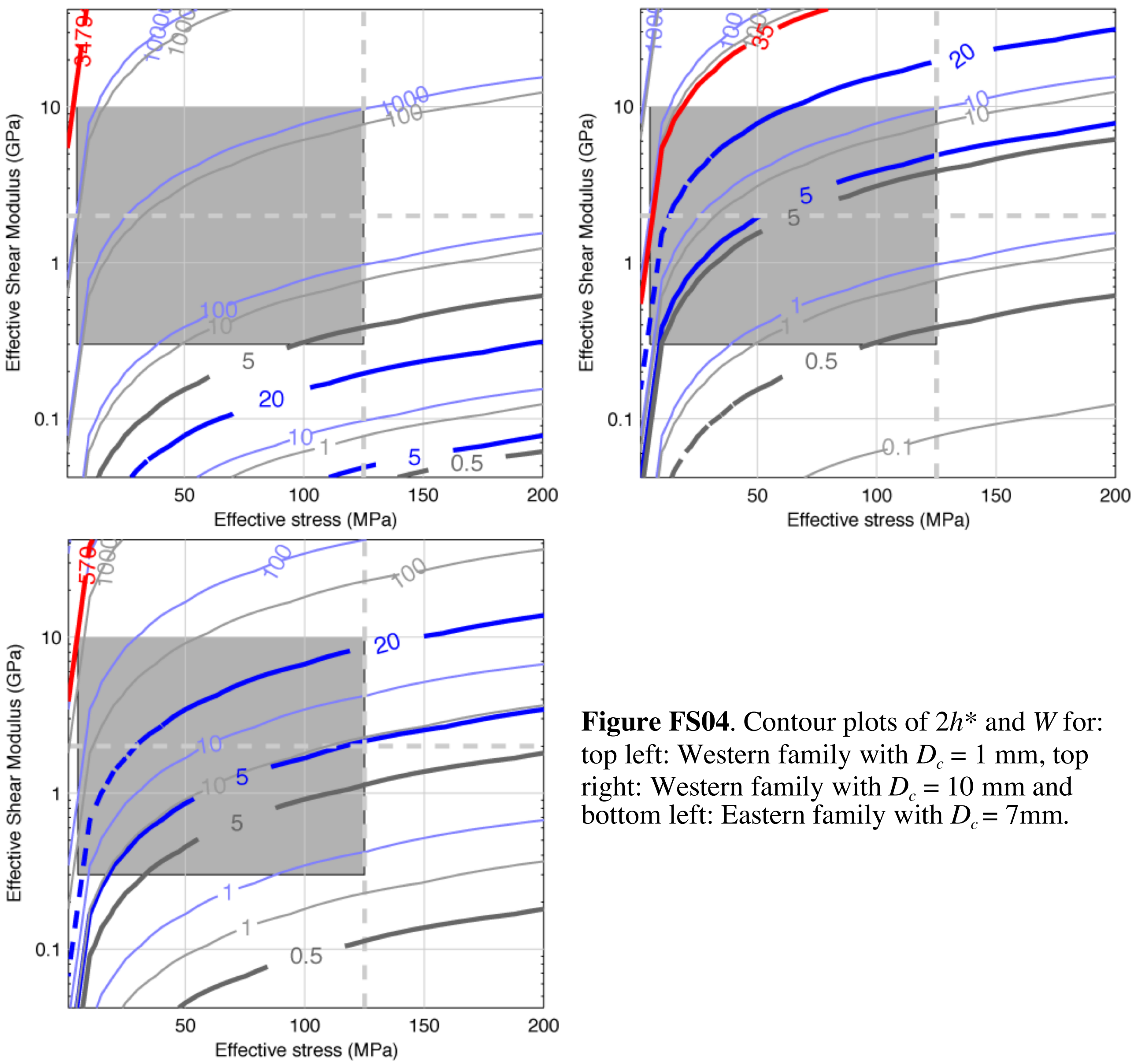

Figure FS04. Contour plots of $2h^*$ and W for: top left: Western family with D_c = 1 mm, top right: Western family with D_c = 10 mm and bottom left: Eastern family with D_c = 7mm.

From (1), the choice of D_c fixes *(b-a),* which appears in all length scale definitions. In order to produce consistent length scale values, where $2h^* < W$, we require $D_c < 7.9$ mm (Auxiliary Material Figure FS04). This is two to three orders of magnitude greater than the 10-100 μm range measured in laboratory experiments, but for those values, given south flank length-scales and pressures, *G'* is implausibly low: ≤ 1 MPa. Increasing D_c to the mm range, consistent with some modeling and in-situ attempts to estimate the parameter [e.g. *Marone et al.*, 2009], satisfies the length constraints while requiring values for *G*' on the order of 2 GPa (Figure 4). Although still unusually low, this is within a plausible range (see Auxiliary Material for more discussion). Alternatively, the *G'* we are constraining may reflect the fault zone material itself where low values are expected for fault gouge.

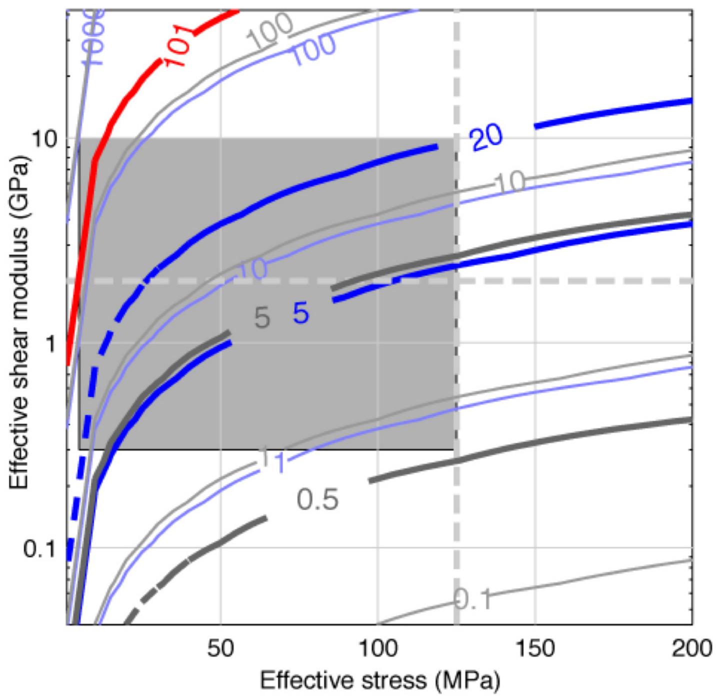

Figure 4. Contours of length scales $2h^*$ (gray) and W (blue) for mean WF SSE, with respect to σ_e and *G'* for $D_c = 7$ mm and $(b-a) = 5.9 \times 10^{-5}$. Light gray box indicates most plausible range for σ_e (5–125 MPa) and *G'* (0.3–10 GPa). Heavy gray contours: $2h^*$=0.5 and $2h^*$=5 km; heavy blue contours: W=5 and W= 20 km. To satisfy length constraints, blue contours must be below the gray ones. At most plausible values (heavy dashed light gray lines) of *G'* (2 GPa) and σ_e (125 MPa; p = hydrostatic), $h^* <$ 2.5 km and $W \approx$ 5 km.

With these parameter values and setting D_c = 7 mm, the characteristic repeat time for the WF gives $(b-a) = 5.9\text{x}10^{-5}$, a small but not unreasonable value, and L_∞ =101 km. For the EF, the $2h^*$ < W constraint requires $D_c \leq 3.7$; using 3.5 mm and setting u_{SSE} = 0.02 and Tc = 642, L_∞ = 285 km $(b-a) = 2.5\text{x}10^{-5}$ (see supporting information for more discussion).

5. Discussion

For both SSE families this analysis predicts L_∞ would be considerably larger than the scale of the south flank. This implies the SSEs will never accelerate to EQ rupture speeds and that large EQs must nucleate elsewhere beneath the flank where frictional properties are more conducive to their generation. For L_∞ to be smaller than the available fault length for the observed seismic portion of the decollement (Figure 1), assuming the same *G'* and D_c = 7 mm, $(b-a) \approx 1.5\text{x}10^{-4}$: several times higher than in the SSE region to the west.

Interestingly, σ_e is required to be high, with pore-pressures of the same order as the hydrostatic pressure. Otherwise at our length-scale range, *G'* once again would be implausibly low. For SSEs occurring on megathrusts within subduction zones, non-volcanic tremor is strongly correlated with the events. R&S theory for those conditions predicts high pore-fluid pressures are required, while petrological transitions exist at the relevant pressures and temperature that involve dewatering. Although the smectite to illite transition is possible at the pressure and temperature conditions under Kilauea's south flank, and compaction could be an active process, the high σ_e our results predict for plausible values of G' suggests there are no high- pressure pore fluids on the section of the fault slipping during the SSEs. This is consistent with the lack of any tectonic tremor detected to date during these events [*Montgomery-Brown et al.*, 2013].

Acknowledgments. We thank Asta Miklius and the Hawaiian Volcano Observatory, and Paul Segall for the interchange of GPS data which are made publicly available via UNAVCO.

References:

Brooks, B. A., J. H. Foster, M. Bevis, C. Wolfe, and M. Behn (2006), Periodic slow earthquakes on the flank of Kilauea volcano, Hawai'i, Earth Planet. Sci. Lett., 246, 207-216.

Brooks, B. A., J. Foster, D. Sandwell, C. J. Wolfe, P. Okubo, M. Poland, and D. Myer (2008), Magmatically Triggered Slow Slip at Kilauea Volcano, Hawaii, Science, 321, 1177, doi: 10.1126/science.1159007.

Cervelli, P., P. Segall, K. Johnson, M. Lisowski, and A. Miklius (2002), Sudden aseismic fault slip on the south flank of Kilauea Volcano, Nature, 415(6875), 1014-1018.

Davis, E., M. Heesemann, and K. Wang (2011), Evidence for episodic aseismic slip across the subduction seismogenic zone off Costa Rica: CORK borehole pressure observations at the subduction prism toe, Earth Planet. Sci. Lett., 306(3-4), 299-305, doi: 10.1016/j.epsl.2011.04.017.

Liu, Y., and J. R. Rice (2005), Aseismic slip transients emerge spontaneously in 3D rate and state modeling of subduction earthquake sequences, J. Geophys. Res., 110(B08307), 14pp, doi: 10.1029/2004JB003424.

Liu, Y., and J. R. Rice (2007), Spontaneous and triggered aseismic deformation transients in a subduction fault model, J. Geophys. Res., 112(B9), B09404, doi: 10.1029/2007jb004930.

Lowry, A. R. (2006), Resonant slow fault slip in subduction zones forced by climatic load stress, Nature, 442(7104), 802-805, doi: 10.1038/nature05055.

Marone, C., M. Cocco, E. Richardson, and E. Tinti (2009), The critical slip distance for seismic and aseismic fault zones of finite width, International Geophysics, 94, 135-162.

Montgomery-Brown, E. K., P. Segall, and A. Miklius (2009), Kilauea slow slip events: Identification, source inversions, and relation to seismicity, J. Geophys. Res., v. 114(no. B6, B00A03), 20 p, doi: doi:10.1029/2008JB006074.

Montgomery-Brown, E. K., C. H. Thurber, C. J. Wolfe, and P. Okubo (2013), Slow slip and tremor search at Kilauea Volcano, Hawaii, Geochem. Geophys. Geosyst., v. 14(no. 2), p. 367-384, doi: doi:10.1002/ggge.20044.

Montgomery-Brown, E. K., D. K. Sinnett, M. Poland, P. Segall, T. Orr, H. Zebker, and A. Miklius (2010), Geodetic evidence for en echelon dike emplacement and concurrent slow slip during the June 2007 intrusion and eruption at Kīlauea volcano, Hawaii, J. Geophys. Res., v. 115(B07405), 15 p, doi: doi:10.1029/2009JB006658.

Owen, S., R. Denlinger, M. Sako, P. Segall, M. Lisowski, and A. Miklius (2000), Rapid deformation of Kilauea Volcano: Global Positioning System measurements between 1990 and 1996, J. Geophys. Res., 105(8), 18,983-918,998.

Perfettini, H., and J. Schmittbuhl (2001), Periodic loading on a creeping fault: Implications for tides, Geophys. Res. Lett., 28(3), 435-438, doi: 10.1029/2000gl011686.

Perfettini, H., J. Schmittbuhl, J. R. Rice, and M. Cocco (2001), Frictional response induced by time-dependent fluctuations of the normal loading, J. Geophys. Res., 106(B7), 13455-13472, doi: 10.1029/2000jb900366.

Rice, J. R. (1993), Spatio-temporal complexity of slip on a fault, J. Geophys. Res., 98(B6), 9885-9907.

Rubin, A. M. (2008), Episodic slow slip events and rate-and-state friction, J. Geophys. Res., 113(B11), B11414, doi: 10.1029/2008jb005642.

Rubin, A. M. (2011), Designer friction laws for bimodal slow slip propagation speeds, Geochem. Geophys. Geosyst., 12(4), Q04007, doi: 10.1029/2010gc003386.

Rubin, A. M., and J. P. Ampuero (2005), Earthquake nucleation on (aging) rate and state faults, J. Geophys. Res., 110(B11), B11312, doi: 10.1029/2005jb003686.

Schwartz, S. Y., and J. M. Rokosky (2007), Slow slip events and seismic tremor at circum-Pacific subduction zones, Rev. Geophys., 45(3), RG3004, doi: 10.1029/2006rg000208.

Segall, P., A. M. Rubin, A. M. Bradley, and J. R. Rice (2010), Dilatant strengthening as a mechanism for slow slip events, J. Geophys. Res., 115(B12), B12305, doi: 10.1029/2010jb007449.

Segall, P., E. K. Desmarais, D. Shelly, A. Miklius, and P. Cervelli (2006), Earthquakes triggered by silent slip events on Kilauea volcano, Hawaii, Nature, 442(6), 71-74, doi: 10.1038/nature04938.

Auxiliary Material

S1. Data & Methods

S1.1 GPS data

We processed daily batches of 30s sampled GPS observations using the GAMIT processing package, with several Pacific-region IGS sites included along with the ~45 Hawaii sites, divided in two processing subnets. Precise orbits and Earth orientation parameters from MIT were used, and predicted Earth-tidal components were applied. We estimated hourly tropospheric delays. GLOBK was used to merge the subnets and a network adjustment routine [e.g. *Caccamise et al.*, 2005] was applied to estimate and remove regional network common-mode error and, by constraining the velocities of a selection of well-behaved stable sites, transform the resulting time-series into a Pacific-plate-fixed reference frame.

S1.2 Step estimation

The SSEs produce seaward steps in the GPS displacement time series. These steps were estimated by fitting Heaviside functions to the time-series using a robust least squares approach. In most cases a 160-day data window was adopted, and a linear velocity simultaneously estimated. However, for a few SSE dates, at a subset of GPS sites, magmatic events introduce complex rate changes to the time series. For these events, smaller time windows and/or a change in velocity were used to more accurately model the time series and estimate the SSE displacements.

S1.3 Correlation Filter Analysis

The reference event for each family is created by normalizing each of the family's known events to the sum of the magnitudes of the slip vectors for those GPS sites that were recording data in all events, and then calculating the mean three-dimensional normalized displacement at each site. Incremental displacements are estimated by fitting steps at each epoch, using the same piecewise constant model used to determine the SSE offsets, though with a shorter, 40-day, data window to minimize artifacts from magmatic events.

S1.4 Slip Distribution

We use a depth of 7.5 km for the decollement below the south flank, a strike of 240° and a dip of 2° to the northwest, and invert for the amount of up-dip slip on discrete fault patches that best fits the observed GPS site displacements. In order to constrain the problem a Laplacian smoothing approach is adopted, with a smoothing factor of 0.003 (see Auxiliary Material Figure FS03) chosen as representing the best trade-off between model smoothness and minimizing displacement residuals. The slip on each discrete fault patch (where bold indicates a vector or matrix quantity), is given by

$$\begin{bmatrix} \boldsymbol{WG} \\ k\Delta \end{bmatrix} \boldsymbol{X} = \begin{bmatrix} \boldsymbol{Wd} \\ 0 \end{bmatrix},$$

where $\boldsymbol{W}$ is a weight matrix formed from the inverse variances of the GPS displacement errors, $\boldsymbol{G}$ is the matrix of Green's functions describing the motion at each GPS site due to slip on each patch, k is the smoothing factor, $\boldsymbol{\Delta}$ is the Laplacian matrix, and $\boldsymbol{d}$ is the vector of observed GPS site displacements.

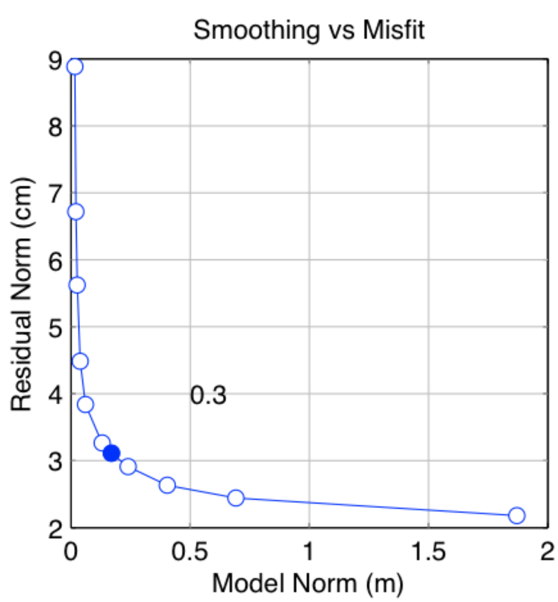

Figure FS03. L-curve of model norm vs residual norm. Value of 0.3 cm/m (= 0.003 m/m) was chosen as the best compromise for scaling the Laplacian smoothing in the slip distribution inversion.

S2. South Flank Shear Modulus

Laboratory measurements of *G'* for hand-sample size pieces of Hawaiian basalt found values ranging from 13 to 23 GPa [*Manghnani and Woollard*, 1966]. These values likely represent a high upper limit given the extensive fracturing of the volcanic edifice. An estimate of *G'* for the top few km of the rift zone using geodetic data found values of 3-9 GPa [*Rubin and Pollard*, 1987]. With the upper half of the submarine flank composed largely of loosely consolidated debris [Morgan et al., 2000; 2003], it is therefore not implausible to expect *G* here to be even lower still.

Using empirical relationships derived by rock engineers [*Hoek and Brown*, 1997; *Hoek and Diederichs*, 2006], a value for *G* that is representative for deformation can be estimated based on the strength of the constituent material and its structure. Basalt is considered very strong, with a uniaxial compressive strength 100-250 MPa. As the ocean-lava interactions responsible for the off-shore debris likely produce relatively weak rocks we consider the lower end more representative. For a poorly interlocked, heavily broken, rock mass of rough, fresh material, with a mixture of angular and round pieces, a “Geological Strength Index” of 40-50 is listed, which predicts a “deformation” shear modulus of 2.2-4.0 GPa.

Closer to the fault surface, fractures and void space should have mostly closed, and 2 GPa for typical rock densities would imply a shear wave velocity of ~850 m/s. At 7.5 km depth that would be unusually low. It is possible however that the relevant G' here is the G' on the fault, and not the G' of the volume surrounding it.

Table TS01. Catalog of identified slow slip events, their recurrence intervals (days) and their estimated equivalent moment magnitudes (using G = 20/2 GPa).

Western Family			**Eastern Family**		
Date	***Int.***	M_w	***Date***	***Int.***	M_w
20-Sep-1998		5.6/5.1	01-Mar-1998		5.3/4.6
09-Nov-2000	781	5.7/5.1	20-Nov-1999	629	5.5/4.7
16-Dec-2002	767	5.5/4.8	04-Jul-2003	1322	5.4/4.6
26-Jan-2005	772	5.8/5.2	17-Sep-2008	1902	5.3/4.6
18-Jun-2007	873	*5.7/5.1*			
31-Jan-2010	958	5.8/5.4			
31-May-2012	851	5.9/5.3			

Table TS02. Parameters used, with assumed values, ranges or estimated values.

Parameter	**Value/Range**	**Notes**
b	0.01	Assumed
ν	0.25	Assumed
u_{SSE}	0.06/0.02 m	Mean west/east family fault slip
V_{creep}	0.25 m.yr^{-1} (8x10^{-9} ms^{-1})	Mean decollement slip rate
V_{SSE}	0.06/0.02 m.day^{-1} (6x10^{-7}/36x10^{-7} ms^{-1}	Mean west/east family SSE slip rate
σ_n	200 MPa	Lithostatic pressure at ~7.5 km decollement depth
p	0-200 MPa	Pore pressure range (no fluid -> lithostatic pressure)
σ_e	0-200 MPa	Effective normal stress = $\sigma_n - p$
L_∞	20+ km	Minimum (2L_∞) patch size for instability

G/G'	.1-10 GPa	Shear modulus/Effective ($G'=G./(1-\nu)$) shear modulus (best estimate =2 GPa)
$b-a$ (a)	$2\text{x}10^{-6}$	
D_c	0.007 m	Characteristic slip distance for state evolution
T_c	834/624 days	Characteristic recurrence time (west/east family)
h^*	0.25 – 2.5 km	Plausible range for minimum half-length for slip nucleation
W	5 – 20 km	Length of SSE slip patch